JET INTERACTING WITH VEGETATION IN A ROTATING BASIN

Francesca De Serio (1), Elvira Armenio (2), Gualtiero Badin (3), Alice Di Leonardo (4), Roni Hilel Goldsmith (5), Dan Liberzon (5), Michele Mossa (2), Eletta Negretti (6), Giuseppe R. Pisaturo (7), Maurizio Righetti (7), Joel Sommeria (6), Donatella Termini (4), Thomas Valran (6), Bart Vermeulen (8) & Samuel Viboud (6)

(1) CoNISMa, National Interuniversity Consortium for Marine Sciences, Italy, E-mail: francesca.deserio@poliba.it
(2) Polytechnic University of Bari, Italy, E-mail: elvira.armenio@poliba.it; michele.mossa@poliba.it
(3) Universitat Hamburg, Germany, E-mail: gualtiero.badin@uni-hamburg.de
(4) University of Palermo, Italy, E-mail: alice.dileonardo@unipa.it; donatella.termini@unipa.it
(5) Technion, Israel, E-mail: ronihilel@gmail.com; liberzon@technion.ac.il
(6) LEGI-Grenoble, France, E-mail: joel.sommeria@legi.cnrs.fr; Maria-Eletta.Negretti@legi.cnrs.fr; samuel.viboud@legi.grenoble-inp.fr; Thomas.Valran@legi.cnrs.fr;
(7) University of Bozen, Italy, E-mail: gr.pisaturo@unitn.it; Maurizio.Righetti@unibz.it
(8) University of Twente, The Netherlands, E-mail: b.vermeulen@utwente.nl

Contaminants, nutrients and sediment particles flow into inland and coastal water bodies often forming turbulent jets. The aim of the present research is to improve our capability to describe how jets interact with the environment they discharge into, providing useful insights for possible mitigation of undesired and harmful impacts. Here, we focus on the case of a jet interacting with an obstructed flow under the effect of the Coriolis force as is often the case with large scale rivers discharging into the sea in vegetated environments.

1. INTRODUCTION

Rivers and waste water flowing into lakes and coastal waters have a profound effect on aquatic ecosystems, due to transport of turbulence, scalars (tracers) and sediment particles. The mixing and spreading of the outflow have an even greater impact when vegetation canopies or mussel cultivation farms occupy the receiving site. Thus, a thorough knowledge of the interaction between effluents and receiving environments is required, to mitigate undesired impacts and to develop best environmental management practices, also highlighted in the recent EU Marine Strategy Framework Directive (2015).

Mixing processes induced by the inflow of unobstructed jets are rather well understood, and are mainly governed by the initial jet characteristics, the boundary conditions and the hydrodynamic features of the ambient current (Nepf, 2012; Smith & Mungal, 1998; Liberzon & Fernando, 2014). When discharging in the presence of rotation, the Coriolis force changes the orientation of turbulent eddies, affecting the energy cascading process (Lin & Atkinson, 1999). For density driven jets (Thomas & Linden, 2007; Cenedese & Adduce, 2008), mixing and entrainment depend on bottom slope, Froude and Reynolds numbers.

Our knowledge of the effect of vegetation on flows in general is rather extensive. The vegetation canopy, characterized particularly by its density and geometry (Oldham & Sturman, 2001; Nepf et al. 1997; Ghisalberti & Nepf, 2005; Poggi et al., 2009; Nepf, 2012; Termini, 2015), interacts with the mean and turbulent flow, perturbing both advection and dispersion (Raupach & Thom, 1981; Ben Meftah et al., 2015; De Serio et al., 2018; Righetti, 2008). For canopy flows, the formation of coherent structures has been studied also numerically by e.g. Bailey & Stoll (2016). Momentum jets obstructed by vegetation have been investigated only recently (Ben Meftah et al., 2015; Ben Meftah & Mossa, 2016). It is well known that, when released in an unobstructed flow, the momentum jet experiences entrainment, while detrainment is observed for density jets. Results by Mossa & De Serio (2016) and Mossa et al. (2017) showed that the vegetation canopy is capable of inducing detrainment for momentum jets, which is an unexpected behavior. Although there is quite a good understanding of turbulent jets interacting with rotating frames and with

vegetation in isolation, to the best of our knowledge experimental investigation of jets released in a vegetated pattern under the effect of the Coriolis force was never reported. This motivated the present study.

In the ocean, the direct effect of rotation on turbulence induced by an obstructed pattern should be quite negligible, because of its small scale. Nevertheless, the mean flow is modified by rotation and consequently the transport and spreading of turbulent kinetic energy and tracers by the mean flow is modified in a rotating frame (Godeferd & Moisy, 2015). Furthermore, the rotational effects are manifested through the development of Ekman boundary layers, effectively increasing friction. Hence, the interplay between rotation and turbulence due to obstacles deserves a thorough study.

It is worth noting that obstructions for the jet discharge are not only representative of vegetated canopies, but also include mussels or oyster cultivation farms and mangrove forests in coastal regions. Therefore, the results of such experiments are expected to support environmental planning. Here, we report the experimental setup and methods and the very preliminary results, focusing on the average velocity, vorticity and turbulence as observed under various experimental conditions.

2. EXPERIMENTAL SETUP

The experiments were carried out in the Coriolis rotating platform at LEGI-Grenoble. In this large-scale facility, two different kinds of experiments were executed, discharging a horizontal momentum jet 1) in the unobstructed tank; 2) in the tank partially obstructed by a canopy made of rigid rods. In the first case, the jet (mimicking a generic discharge) spread and transport in a rotating background were examined. In the second case, the outflow spread through the obstructed pattern in a rotating background was investigated. Both experiments were conducted under identical rotation parameters expressed by T, the rotation period of the tank: $T=\infty$ (no rotation), T=60s T=90s, T=120s and T=180s. Some parameters, such as the spacing s between the rods and the jet initial flowrate q_j, were varied during the tests to evaluate their effects on the jet behavior. In this report, we show the preliminary results of some of the experimental runs.

The LEGI tank has a diameter of D=13m, the working water depth was set at H=0.80m. A dedicated pipework, installed in the tank, was used to release the momentum jet. The pipe outlet O was 0.10m in diameter, rigidly fixed at 0.40m depth. The outlet ensured a horizontal release of a jet with an initial diameter of d_j=0.08m (internal diameter of the pipe) oriented horizontally. A specially designed canopy was placed in the tank for the obstructed configuration. The rigid, emergent vegetation stems were mimicked by plastic transparent (Plexiglass made) rods of diameter d=0.02m, arranged on a 2m x 2m panel fixed at the bottom of the tank. The rods were manually mounted on the panel inside pre-drilled holes, thus assuring a regular pattern with a center-to-center distance s. The panel was placed in the tank as shown in Figure 1, between the carriage supports, which also proved a positioning platform for the instruments. The center of the jet outlet (O) was 1m away from the upstream edge of the panel and 0.77m from its external edge.

The instantaneous measurements of the velocity field at several pre-selected horizontal planes were principally made using a PIV (Particle Image Velocimetry) system. The laser source of the PIV system was mounted in the center of the tank, and the system included three synchronized recording cameras mounted on the top of the tank. The laser used in our experiments was a continuous Yag laser (532 nm wavelength) providing 25 Watts of power, illuminating a large area of the rotating tank by a horizontal sheet. A Powell prism produced the 5mm thick sheet. In the measurements discussed here, the laser sheet was set in a horizontal plane spanning an area of more than 3x3 m^2, with a 60° opening angle. Orgasol neutrally buoyant particles with a 60µm diameter were used to seed the flow. To map the velocity fields in the examined volume of water a "multi-level" approach was adopted, acquiring several images and consequently the 2D velocity fields at each horizontal layer of interest. See Figure 2 to have a view of the set up. Figure 3 shows, as an example, the six horizontal layers measured by the PIV during each experiment. These are named as 0, m1, m2, 1, 2, 3, respectively for z=0m, -0.10m, -0.2m, 0.1m, 0.2m, 0.3m,

being *z* the vertical axis, positive upward, with origin at the jet outlet. The rigid rods are also sketched in this figure.

The three cameras, named PCO1, PCO2 and Falcon, were fixed on rigid supports located at 4.29m, 4.74m, and 4.87m from the bottom, respectively. PCO1 and PCO2 filmed at 2560 x 2160 pixels resolution using a 35 mm objective lens (Samyang F1.4). The FALCON provided images at 2432 x 1728 pixels resolution using a 20mm objective lens (Sigma F1.8). Orientation of the cameras ensured the three fields of view partially overlapped, in order to ensure full coverage of the deviated jet (Figure 4).

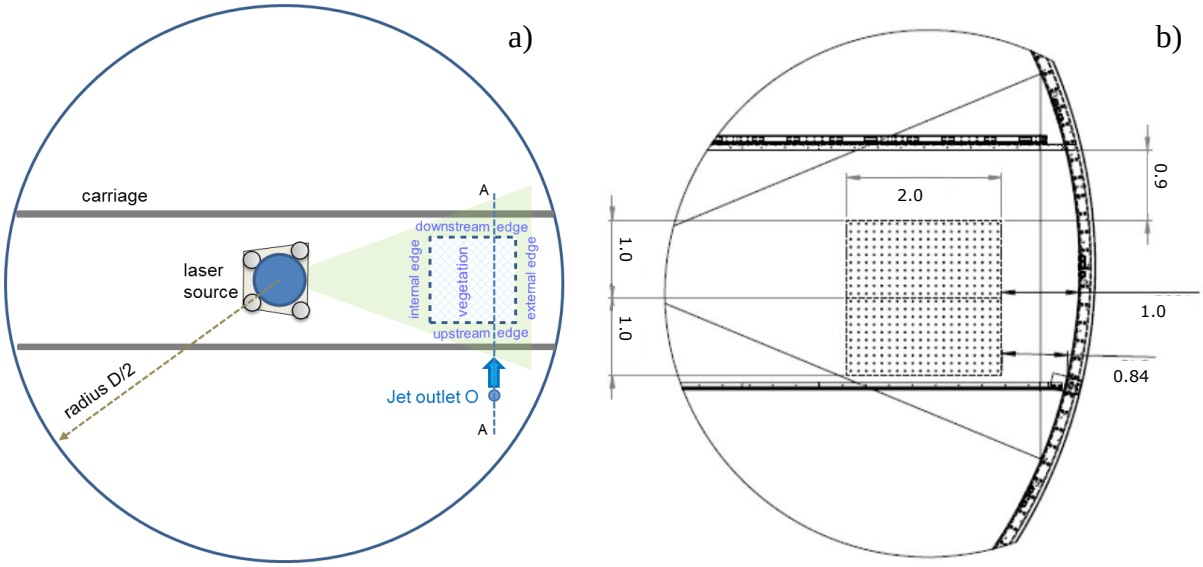

Figure 1. a) Plan view: sketch of the location of jet outlet and vegetation panel in the LEGI tank. b) Detail of the vegetated panel with distances (in m) from the carriage and the tank wall

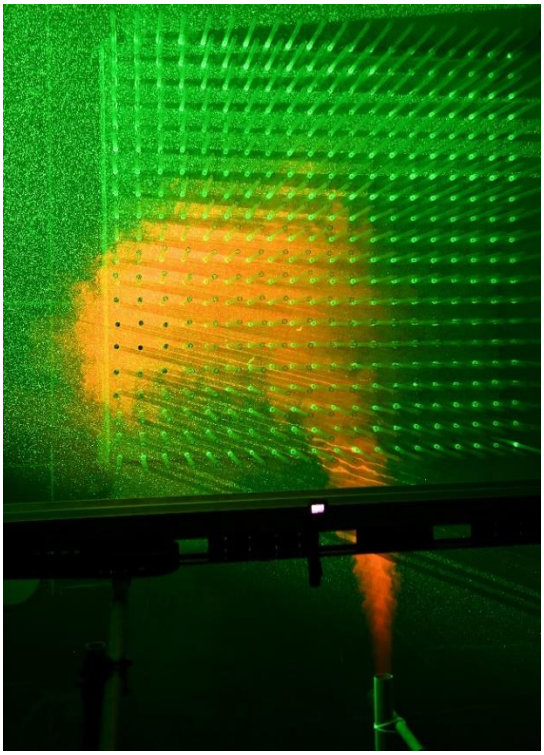

Figure 2. Top view of the experiment set up: dyed jet spreading in the obstructed panel, illuminating by the laser. Jet outlet position as in Fig.1a)

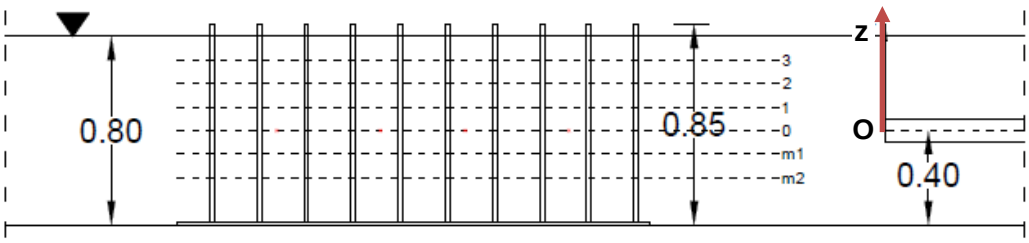

Figure 3. View in the vertical plane (AA dotted line in Fig.1a) of the investigated layers at different depths (measurements in m). Dashed lines are reciprocally distant 0.10m

In addition to the PIV system described above, some velocity measurements were also carried out by means of two 3D Acoustic Doppler Velocimeters (3D-ADV), a bottom-looking one and a side-looking one. The ADVs provided velocity measurements with accuracy of ±0.5% of measured value ±1 mm/s. Settled with a sampling frequency of 50Hz, the ADVs required a measurement time equal to 2-3 minutes to obtain a satisfactory signal. Independently from the obstacles, such measurement times were not possible as the released jet travels through the entire tank coming back to its origin, thus overlapping with itself. This behavior was noted at preliminary testing using a dyed jet visualization. In both unobstructed and obstructed cases, the ADV measurements at several locations at selected depths were hence used to check the spreading of the jet in the still water, to compare it with the expected theoretical trend and previous research result, which were confirmed.

Table 1 lists the experimental parameters (not significant EXPs are not listed). After the preliminary tests (denoted as EXP1 to EXP13), the main 14 experimental runs were conducted (EXP14 to EX27) using the PIV system as described above. Five additional experiments (denoted EXP28 to EX32) were conducted implementing the volume scanning technique. Here the LIF (Laser Induced Fluorescence) system scanned the target volume rapidly, recording images of the water motion seeded with a fluorescent dye (Rhodamine 6G). The laser was scanning vertically in order to provide detection of the jet volume and to support reconstruction the jet three-dimensional shape. These results will not be reported here as the data is yet to be processed.

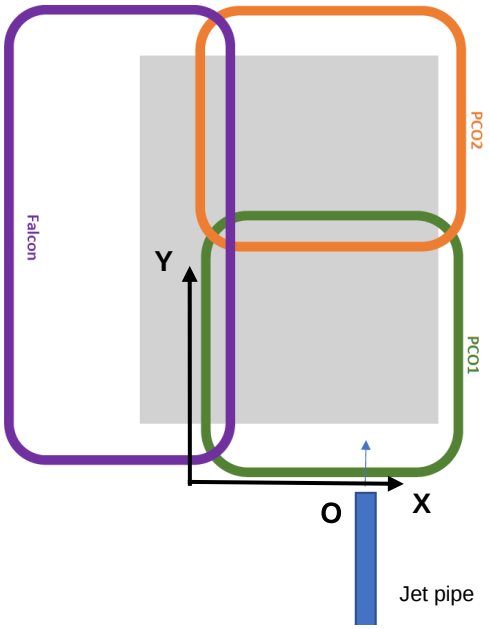

Figure 4. Sketch of the frames in the horizontal plane covered by the three top cameras used in the PIV system. Coordinate reference system for PCO1 shown.

EXP number	T [s]	Vegetation spacing *s* [cm]	Jet flowrate q_j [m^3/h]	Instruments used
EXP2	No rotation	unobstructed	20.7	ADVs
EXP7	No rotation	20	20.7	ADVs
EXP9	60	20	20.7	ADVs
EXP13	90	unobstructed	20.7	PIV
EXP14	No rotation	unobstructed	20.7	PIV
EXP15	90	Unobstructed	20.7	PIV
EXP16	60	Unobstructed	20.7	PIV
EXP17	No rotation	20	20.7	PIV
EXP18	60	20	20.7	PIV
EXP19	90	20	20.7	PIV
EXP20	120	20	10.8	PIV
EXP21	No rotation	20	20.7	PIV
EXP22	No rotation	10	20.7	PIV
EXP23	90	10	20.7	PIV
EXP24	60	10	20.7	PIV
EXP25	120	10	10.8	PIV + ADVs
EXP26	180	10	10.8	PIV + ADVs
EXP27	No rotation	10	10.8	PIV + ADVs
EXP28	No rotation	10	20.7	LIF
EXP29	90	10	20.7	LIF
EXP32	60	10	20.7	LIF

Table 1. List of the principal executed experiments, with different configurations

3. DATA PROCESSING

The mode of operation for each of the PIV supported experiments was as follows. The horizontal layer under consideration was illuminated with the laser sheet, and simultaneously filmed by the three PIV cameras. Each camera was filming at 33Hz (i.e. frame time of 0.03s) for the duration of 1 minute, thus providing a total of 2000 images. The images were successively coupled and correlated, to obtain the PIV measured velocity field in the horizontal plane. As for the PIV images, we adopt a coordinate reference system (X,Y) which refers to the frame, with the X axis aligned with the panel upstream edge and positive outwards, while the Y axis is aligned with the internal edge and positive in the jet direction (see Fig. 4). Velocities in the X direction are named u, while those in the Y direction are named v.

The open source ParaPIV software (Wang, 2017) running in Matlab 2017b was used to process the acquired images. Extensive parallelization (16 cores) was implemented to reduce computational times. The PIV results presented below were obtained using a 16 X 16 pixels interrogation window. The calibration coefficients were estimated taking EXP 27 as a reference (see Table 1) and are shown in Table 2. For each horizontal layer of each experiment a time series of velocity data on a grid with 159x134 points in the case of both PCO1 and PCO2 and 151x107 points in the case of Falcon camera were obtained.

Layer	PCO1 [cm px^{-1} s^{-1}]	PCO2 [cm px^{-1} s^{-1}]	Falcon [cm px^{-1} s^{-1}]
0	2.1667	2.4567	3.9633
1	2.1233	2.4267	3.9167
2	2.0933	2.3900	3.8467
3	2.0400	2.3533	3.7767
m1	2.2133	2.5000	4.0433
m2	2.2533	2.5467	4.1033

Table 2. Velocity calibration coefficients

4. FIRST RESULTS AND CONCLUSION

Large number of experimental runs have provided us with a massive data set, which is being processed. Here we present and discuss in brief only the initial results of few selected cases, as acquired by the PCO1 camera only. Specifically, the experiments addressed here are:

- EXP14 - no rotation, no obstructions, jet with q_j=20.7m^3/h;
- EXP21 - no rotation, obstructions spaced at s=20cm, jet with q_j=20.7m^3/h;
- EXP16 - rotation at T=60s, no obstructions, jet with q_j=20.7m^3/h;
- EXP18 - rotation at T=60s, obstructions spaced at s=20cm, jet with q_j=20.7m^3/h.

Figure 5 presents the average velocity distribution (averaged over the total acquisition time of 1 minute) for the four different EXPs listed above. The results are for the horizontal plane at z=0, i.e. halfway the tank's water depth. The velocity fields are quite typical for the different configurations examined. The jet appears being fully developed along the panel, considering the distance of the jet relative to the panel (and thus to the measurement area) being larger than $10d_j$.

In EXP14 the jet is well defined and undisturbed. The jet travels through still water, exhibiting a quite symmetrical spread in the X direction while propagating along Y. In the first half of the panel length, the velocity magnitude along the centerline of the jet is initially lower than expected, since the investigated layer (z=0) is slightly shifted upward with respect to the axis of symmetry of the jet. In the second half, higher velocity values are observed in the fully developed condition and they gradually decrease along the jet path, as expected in the free jet case, due to the entrainment of ambient water.

In EXP16 rotation is present and the jet is released in water in solid body rotation, thus the curvature of the jet path is evident. The structure of the flow remains quite symmetrical relatively to the jet centerline, but the velocity magnitude is slightly lower in the central part than in EXP14. Lateral circulations can be noted, specifically a weak anticlockwise one spanning the outer part of the frame, and a flow drawn by the bending jet in the inner part of the frame, due to entrainment.

Both cases with obstructions (EXP18 and 21) show significant (up to twofold) reduction in jet mean velocity magnitude due to flow blockage by the rods, confirming previous results (Mossa et al., 2017; De Serio et al., 2018). Also worth noting is the smoothing of velocity in the lateral areas. Cases with obstructions, represented by vertical rods, showed harmonic fluctuations of velocity. Origin and nature of such fluctuations are yet to be determined, with vortex shedding or other wake effects being a possible explanation requiring further investigation.

The time-averaged vorticity distributions are presented in Figure 6, following the same scheme of Fig. 5. The typical vortical structure of jets is observed for the unobstructed cases (EXP14 and EXP16), especially along the second part of the panel, with positive and negative vorticity respectively dominating half of the jet and contributing to entrainment. On the contrary, in EXP21 and EXP18 cases, the presence of vertical rods alters the vorticity distribution and, even if the jet pattern is still identifiable, local concentrations of vorticity around and behind the rods seem more pronounced and prevailing. Furthermore, the oscillating velocity induces a disturbance also in these cases.

In Figure 7, the distribution of the time-averaged turbulent Reynolds stresses $\overline{u'v'}$ (apart from $-\rho$, with ρ water density) is shown for the same four experimental cases. In all cases, it is consistent with the map of the time-averaged velocity, presenting higher values of $\overline{u'v'}$ at locations of higher drag, namely in the initial portion of the flow, also confirming previous works (e.g. Ben Meftah et al. 2018). The presence of the rods (EXP21 and EXP18) reduces the Reynolds stresses magnitude with approximately 30%.

It is evident the different behavior of the jet in obstructed/unobstructed configurations as well as in rotating/not rotating mode. Further analysis is ongoing to highlight with more detail the reciprocal effects of jet, obstructions and rotation.

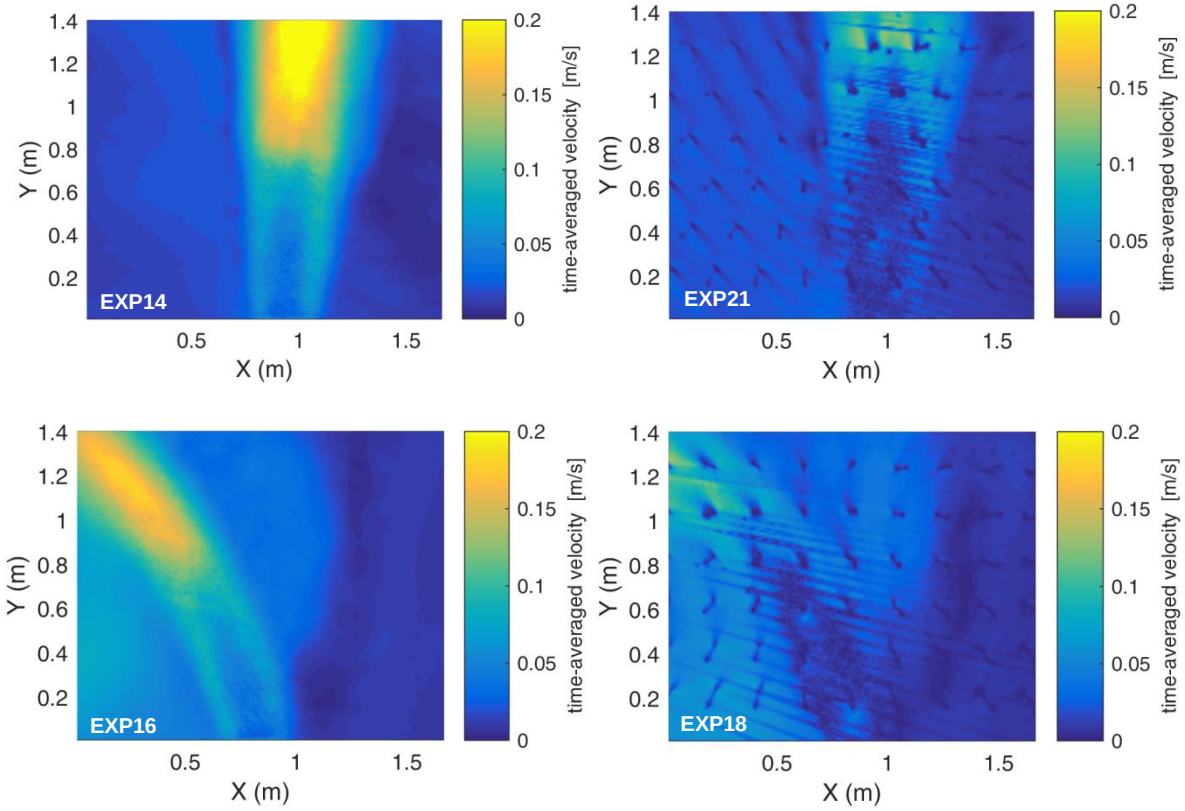

Figure 5. Time-averaged velocities in the horizontal layer at z=0: top line no rotation; left column no obstructions

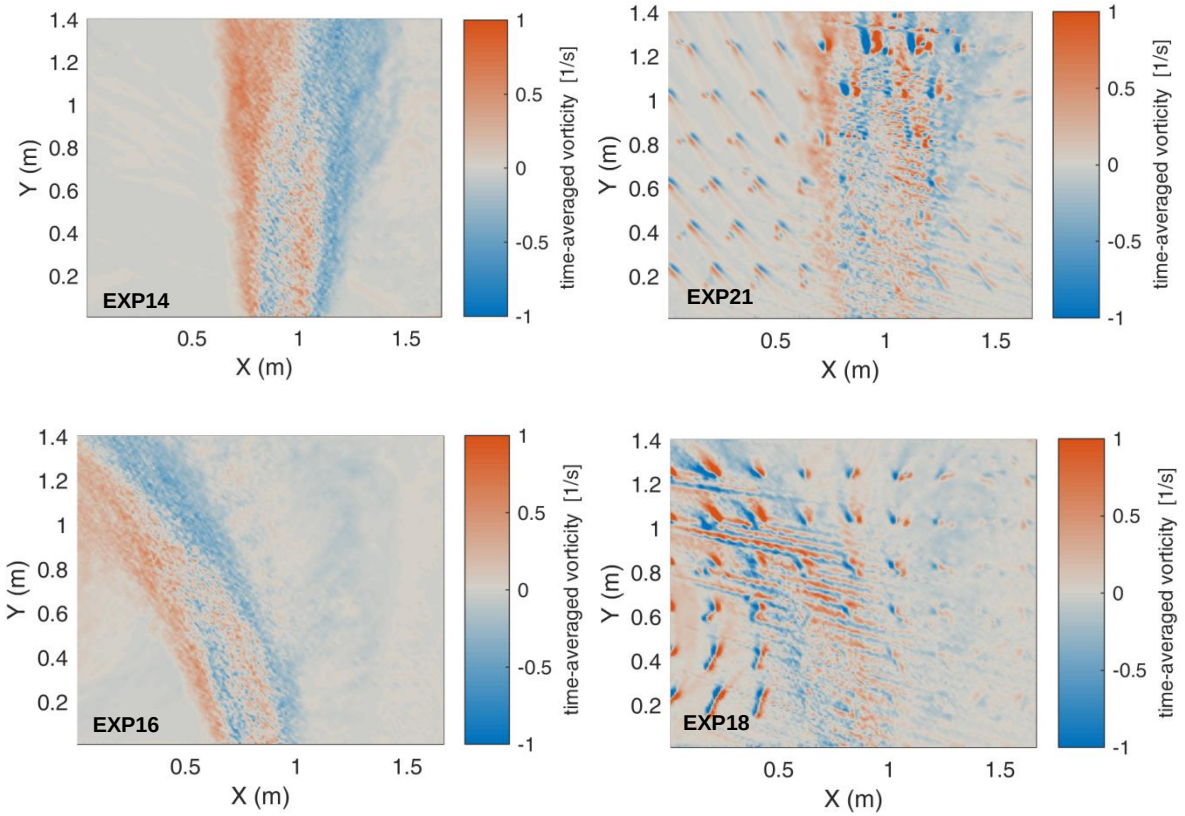

Figure 6. Time-averaged vorticity in the horizontal layer at z=0: top line no rotation; left column no obstructions

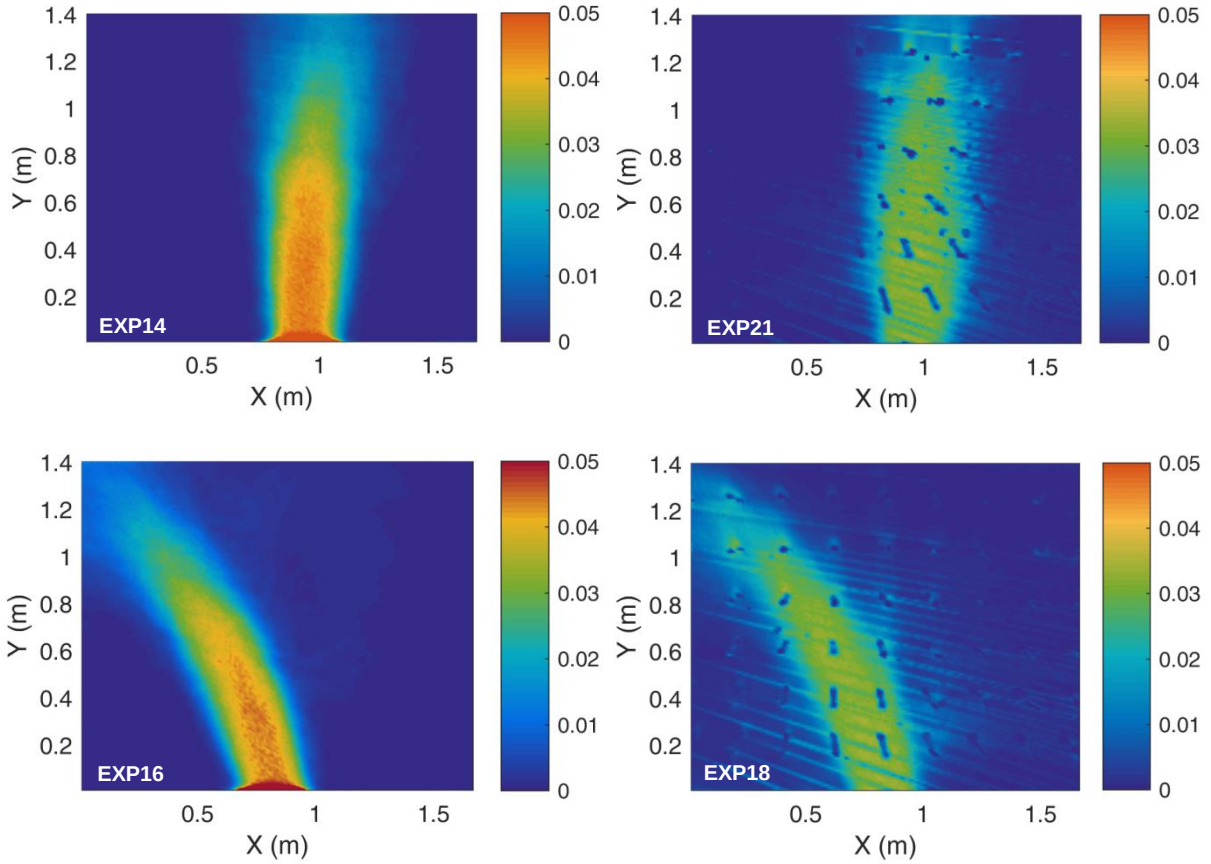

Figure 7. Time-averaged turbulent Reynolds stresses $\overline{u'v'}$ [m^2/s^2] in the horizontal layer at z=0: top line no rotation; left column no obstructions

Acknowledgement

This project (named JEVERB18) has received funding from the European Union's Horizon 2020 research and innovation programme under grant agreement No 654110, HYDRALAB+.

References

Bailey, B.N, and Stoll, R. (2016). The creation and evolution of coherent structures in plant canopy flows and their role in turbulent transport, *J. Fluid Mech.*, 789, 425-460.

Ben Meftah, M., De Serio, F., Malcangio, D., Mossa, M. and Petrillo, A.F. (2015). Experimental study of a vertical jet in a vegetated crossflow, *J. Env. Management,* 9.

Ben Meftah, M. and Mossa, M. (2016). Partially obstructed channel: Contraction ratio effect on the flow hydrodynamic structure and prediction of the transversal mean velocity profile. *Journal of Hydrology,* 542.

Cenedese, C. and Adduce, C. (2008). Mixing in a density-driven current flowing down a slope in a rotating fluid, *J. Fluid Mech.*, 604, 369–388.

De Serio, F., Ben Meftah, M., Mossa, M. and Termini, D. (2018). Experimental investigation on dispersion mechanisms in rigid and flexible vegetated beds, *Advances in Water Resources*, 120, 98-113.

Ghisalberti, M. and Nepf, H. (2005). Mass transfer in vegetated shear flows. *Environ. Fluid Mech.*, 5(6), 527-551.

Godeferd, F.S. and Moisy, F. (2015). Structure and Dynamics of Rotating Turbulence: A Review of Recent Experimental and Numerical Results, *Applied Mechanics Reviews*, 67, 030802-1.

Liberzon, D. and Fernando, H.J.S. (2014). Pressure distribution in confined jet flow, *Journal of Fluids Eng.*, 136, 3, 031202.

Lin, G., Atkinson, J.F. (1999). A Mechanism for Offshore Transport across the Gulf Stream, *J. Phys. Ocean.*, 30, 226-232.

Mossa, M. and De Serio, F. (2016). Rethinking the process of detrainment: jets in obstructed natural flows, *Scient. Rep*., 3910.

Mossa, M., Ben Meftah, M., De Serio, F. and Nepf, H. (2017). How vegetation in flows modifies the turbulent mixing and spreading of jets, *Scient. Rep.*,7, 6587.

Nepf, H., Mugnier, C. and Zavistoski, R. (1997). The effects of vegetation on longitudinal dispersion, *Est. Coast. Shelf Science,* 44, 675-684.

Nepf, H. (2012). Hydrodynamics of vegetated channels, *J. Hydraul. Res.*, 50(3), 262–279.

Oldham, C.E. and Sturman, J.J. (2001). The effect of emergent vegetation on convective flushing in shallow wetlands: Scaling and experiments, *Limnol. Oceanogr.*, 46(6), 1486–1493.

Poggi, D., Krug, C. and Katul, G.G. (2009). Hydraulic resistance of submerged rigid vegetation derived from first-order closure models, *Water Resource Research*, 45, W10442.

Raupach, M.R. and Thom, A.S. (1981). Turbulence in and above plant canopies, *Annual Rev. Fluid Mech.*, 13, 97–129.

Righetti, M. (2008). Flow analysis in a channel with flexible vegetation using double-averaging method, *Acta Geophysica,* 56(3), 801–823.

Smith, S.H. and Mungal, M.G. (1998). Mixing, structure and scaling of the jet in crossflow, *J. Fluid Mech., 357, 83-122.*

Termini, D. (2015). Flexible Vegetation Behavior and Effects on Flow Conveyance: Experimental Observations. *Int. Jour. of River Basin Manag.*, doi:10.1080/15715124.2015.1012519.

Thomas, P.J. and Linden, P.F. (2007). Rotating gravity currents: small-scale and large-scale laboratory experiments and a geostrophic model, *J. Fluid Mech.,* 578, 35–65.

Wang, C.S. (2017). ParaPIV: PIVlab in Parallel, Technical Report, https://doi.org/10.13140/rg.2.2.30705.79203.